





Article

Estimations of Mutation Rates Depend on Population Allele Frequency Distribution: The Case of Autosomal Microsatellites

Sofia Antão-Sousa ^{1,2,3,4,*} , Eduardo Conde-Sousa ^{1,5} , Leonor Gusmão ⁴ , António Amorim ^{1,2,3} 
and Nácia Pinto ^{1,2,6}

- ¹ Instituto de Investigação e Inovação em Saúde (i3S), 4200-135 Porto, Portugal; econdesousa@gmail.com (E.C.-S.); aamorim@ipatimup.pt (A.A.); npinto@ipatimup.pt (N.P.)
² Institute of Molecular Pathology and Immunology, University of Porto (IPATIMUP), 4200-465 Porto, Portugal
³ Faculty of Sciences, University of Porto (FCUP), 4169-007 Porto, Portugal
⁴ DNA Diagnostic Laboratory (LDD), State University of Rio de Janeiro (UERJ), Rio de Janeiro 20550-013, Brazil; leonorbgusmao@gmail.com
⁵ Instituto de Engenharia Biomédica (INEB), 4200-135 Porto, Portugal
⁶ Center of Mathematics, University of Porto (CMUP), 4169-007 Porto, Portugal
* Correspondence: sofias@ipatimup.pt

Abstract: Microsatellites (or short-tandem repeats (STRs)) are widely used in anthropology and evolutionary studies. Their extensive polymorphism and rapid evolution make them the ideal genetic marker for dating events, such as the age of a gene or a population. This usage requires the estimation of mutation rates, which are usually estimated by counting the observed Mendelian incompatibilities in one-generation familial configurations (typically parent(s)–child duos or trios). Underestimations are inevitable when using this approach, due to the occurrence of mutational events that do not lead to incompatibilities with the parental genotypes ('hidden' or 'covert' mutations). It is known that the likelihood that one mutation event leads to a Mendelian incompatibility depends on the mode of genetic transmission considered, the type of familial configuration (duos or trios) considered, and the genotype(s) of the progenitor(s). In this work, we show how the magnitude of the underestimation of autosomal microsatellite mutation rates varies with the populations' allele frequency distribution spectrum. The Mendelian incompatibilities approach (MIA) was applied to simulated parent(s)/offspring duos and trios in different populational scenarios. The results showed that the magnitude and type of biases depend on the population allele frequency distribution, whatever the type of familial data considered, and are greater when duos, instead of trios, are used to obtain the estimates. The implications for molecular anthropology are discussed and a simple framework is presented to correct the naïf estimates, along with an informatics tool for the correction of incompatibility rates obtained through the MIA.

Keywords: microsatellites; STRs; autosomes; mutation rate estimates biases; hidden mutations; dating; evolution



Citation: Antão-Sousa, S.; Conde-Sousa, E.; Gusmão, L.; Amorim, A.; Pinto, N. Estimations of Mutation Rates Depend on Population Allele Frequency Distribution: The Case of Autosomal Microsatellites. *Genes* **2022**, *13*, 1248. <https://doi.org/10.3390/genes13071248>

Academic Editor: Dror Sharon

Received: 1 June 2022

Accepted: 11 July 2022

Published: 14 July 2022

Publisher's Note: MDPI stays neutral with regard to jurisdictional claims in published maps and institutional affiliations.



Copyright: © 2022 by the authors. Licensee MDPI, Basel, Switzerland. This article is an open access article distributed under the terms and conditions of the Creative Commons Attribution (CC BY) license (<https://creativecommons.org/licenses/by/4.0/>).

1. Introduction

Microsatellites (or short tandem repeats (STRs)) have been widely used in a wide range of scientific fields, such as population and forensic genetics, anthropology, and evolution; see, for example, [1–3]. For most of these usages, a critical parameter is required: the (germinal) mutation rate, that is, the frequency of errors in replicating DNA when producing a gamete. In the field of molecular anthropology, for example, microsatellite mutation rates are used to estimate the coalescence time between the alleles of a locus [4], the date of introduction/expansion of a variant in a population [5–8] and a variety of evolutionary events [9,10].

The main mechanism behind length mutations in microsatellites is thought to be the polymerase template slippage [11,12]. DNA strand slippage may transiently occur

during DNA synthesis, which may result in mutant products where repeat units are added or deleted within the microsatellite [11–13]. Several factors influence microsatellite mutation rates, such as the (i) allele length, (ii) repetitive motif size and sequence, and (iii) parental age and gender. Indeed, (i) longer alleles tend to have higher mutation rates [14]; (ii) longer repeats tend to have lower mutation rates and, among those with the same length, mutations vary according to their sequences [15,16]; (iii) older individuals and males present higher mutation rates [17].

Mutations that involve the gain or loss of a single repeat in the transmitted parental allele single-step mutations are assumed to be preponderant over mutations involving the gain or loss of more than one repeat (multistep mutations) [18,19]. Indeed, the most accepted mutational model is the so-called stepwise mutation model (SMM), which considers single-step mutations as the most frequent when compared to multistep mutations [20]. This bias between single and multistep mutations is supported by studies on Y microsatellites, where length mutations are undoubtedly and specifically identified in simple structure markers [21–23]. Under the SMM framework, a single-step mutation is assumed to have occurred whenever this explains the genotypic incompatibility observed in a duo or trio familial configuration. The standard method for estimating microsatellite mutation rates is detecting and quantifying Mendelian incompatibility rates in one-generation family genotypic configurations, considering either the father or the mother and the child (the so-called duos), or considering both parents and the child (trios) [22,24–27]. However, except in the case of simple structure markers in haploid systems [21,28,29], this methodology entails the underestimation of mutation rates, as mutations may not necessarily lead to incompatibilities between parent(s) and child genotypes, originating ‘hidden’ or ‘covert’ mutations [29–32] (see Figure 1 for examples).

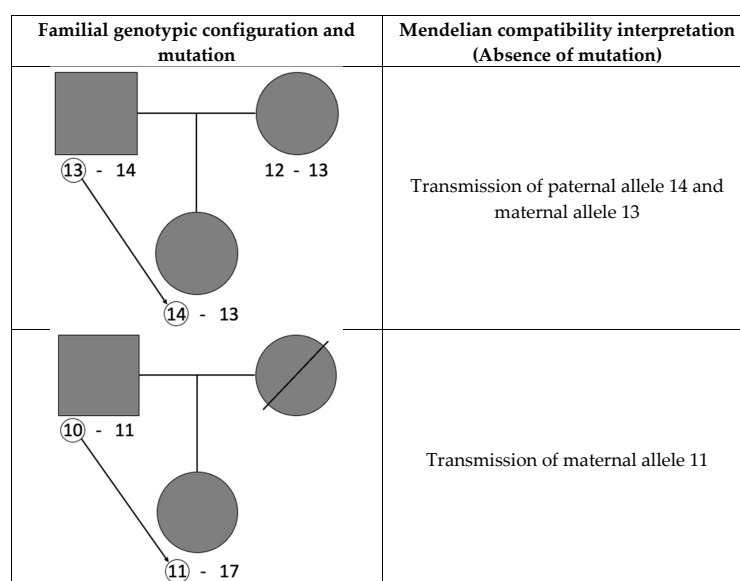


Figure 1. Examples of hidden mutations occurred in a parent–child duo and a parents–child trio, at an autosomal microsatellite. The arrows and circles indicate the allele transmission involving a mutation.

It is known that the likelihood of a mutation resulting in a Mendelian incompatibility is correlated with the type of familial configuration used [28,29], with biases being greater when duos, instead of trios, are analyzed [28–31,33]. A correction method was described previously [29], but the absence of an informatics tool for its implementation may have prevented its use.

In this work, we showed how the magnitude of the underestimation of autosomal microsatellite mutation rates varies with the populations’ allele frequency distribution spectrum, using simulated parent(s)–child duos and trios in different populational scenarios

and assuming single-step mutations. Simulated familial duos and trios were generated considering a single-step mutation for each familial clustering and marker, using real and theoretical mock allele frequency distributions (henceforth called mock). Mock allele frequency distributions were considered to diversify the analyzed population allelic backgrounds and were designed by us considering pre-defined distributions. The populations/markers showing the highest rates of hidden mutations were assumed to be those with the greatest mutation rate biases when a standard approach to quantifying the Mendelian incompatibilities (Mendelian incompatibilities approach (MIA)) is used.

We aim to study the magnitude and type of biases obtained in mutation rate estimates, depending on the population allele frequency distribution and the type of familial data that are considered.

The implications for molecular anthropology are highlighted and a simple framework to correct the naïf mutation estimates, obtained through an analysis of Mendelian incompatibilities, is presented, along with a user-friendly and freely available informatics tool for the corresponding correction of incompatibility rates to mutation rates.

2. Materials and Methods

Familial genotypic configurations, mother–child or father–child duos, and mother–father–child trios, were generated by resorting to Python™ programming language. Since we aimed to measure the proportion of hidden mutations present in different population backgrounds, parental genotypes were randomly attributed from both real and mock population allele frequency distributions. Real allelic distributions concern ten autosomal microsatellites: CSF1PO, D1S1656, D21S11, D2S441, D3S1358, FGA, SE33, TH01, TPOX, and VWA, for the Norway, Somalia, and Spain populations [34]—see Supplementary Material File S1 for a graphic representation of the allelic distributions and Table S1 for population information (size, expected heterozygosity, polymorphism informative content (PIC) allele number, and allelic range). These markers were selected due to their distinct allelic distributions. On the other hand, to diversify the scenarios obtained from real populations and forensic markers, six mock (predefined) frequency distributions were designed by us: normal, bimodal, and constant distributions. For each case, narrow and wide allelic spans (with 10 and 20 alleles, respectively) were considered (Figure 2).

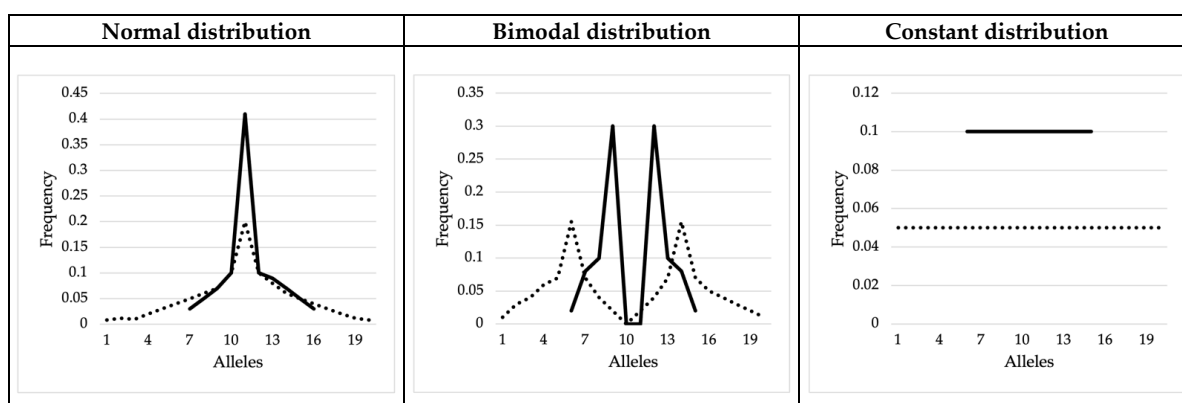


Figure 2. Mock allele frequencies, considering predefined distributions. The full lines correspond to the situation where 10 alleles are considered and the dotted lines to the cases with 20 alleles (narrow and wide distributions, respectively).

Parental genotypic configurations were generated by considering the allele frequencies of Norway, Somalia, and Spain populations [34] and the allele frequencies of the mock distributions (Figure 2). For each marker and population database, 1,000,000 familial genotypic configurations (duos and trios) were simulated, assuming, for each case, the occurrence of exactly one single-step mutation. To simulate the parental alleles, a cumulative relative frequency associated with each allele was considered for each marker. The two and four

parental alleles considered in the case of duos and trios, respectively, were obtained considering two and four, resp., random numbers between 0 and 1. The corresponding allele was then chosen considering this number; the greater the frequency of the allele, the most likely that the allele was selected. When trios were simulated, the meiosis suffering mutation (either paternal or maternal) was randomly selected. Mutated alleles were assumed to be transmitted to the offspring, while the other filial allele was randomly selected either from the population (in the case of duos) or the other parent (in the case of trios).

As a parental mutated allele was assumed to be transmitted to the offspring in all the cases, there were two possible outcomes for each simulated familial configuration: the familial genotypic configuration was incompatible with the Mendelian inheritance, or otherwise. Under the standard, general, approach, the rate of the cases resulting in the first for a specific marker would be presented as the marker specific average mutation rate; while the rate of cases that resulted in the latter equates to the rate of hidden mutations, which would remain unnoticed.

The rate of hidden mutations was quantified for the different markers, populations, and familial configurations, assuming that the higher the rate, the greater the bias of the corresponding marker-specific mutation rate estimated through Mendelian incompatibilities.

Linear regression analyses were performed using Microsoft Excel[®]. The heterozygosity of each marker was calculated as $1 - \sum_i p_i^2$, where p_i is the frequency of the allele i .

Fisher Exact tests to ascertain p values were computed considering a level of significance equal to 0.05. Python algorithms are openly available at <https://github.com/econdesousa/Incomp2Mut.git> (accessed on 23 March 2022), along with an informatics tool.

To replicate the simulations described in this work, and obtain a corrected mutation rate estimate for any marker, population, or familial configuration, the algorithms in <https://github.com/econdesousa/Incomp2Mut.git> (accessed on 23 March 2022) must be run for the target marker and incompatibility rates obtained through MIA. An example file on how to present the allelic distributions and a detailed explanation in video format of how to proceed with the informatic analyses are provided.

3. Results

In this section, results are presented comparing the accuracy of the estimates obtained for autosomal STR mutation rates, considering the analysis of both familial duos and trios, for different markers, populations, and mock allele frequencies, through the evaluation of the hidden mutation rates that were observed—see Table 1 and Figure 3.

3.1. Real Allele Frequency Distributions

As expected, parent–child duos concealed single-step mutations more often than parent–child trios (Table 1). These biases were strongly dependent on the allele frequency distribution of the marker. As a striking example, when considering the population of Norway, the rate of hidden mutations obtained for trios in marker CSF1PO were greater than the one obtained for marker D1S1656 when considering duos. This indicates that, for that population and markers, better estimates are expected for the D1S1656 mutation rate when duos are studied than for CSF1PO when trios are used once the same number of meioses are analyzed. Indeed, within each of the three considered population databases [34], widely different proportions of hidden mutations were found for the 10 analyzed markers, even when the same familial configurations were used (either duos or trios). For example, in parent–child duos, considering the Norwegian database, mutations were concealed 4.3 more often for TPOX than for SE33. Globally, the proportion of hidden mutations varied from 5.4% (in SE33, for the Norwegian population, using trios) to 62.2% (in TPOX, also for the Norwegian population, when using duos). The ratio of hidden mutations found for the 10 analyzed markers in each population was computed. Statistically significant differences were found for virtually all pairwise comparisons; see Supplementary Material File S2. Within all populations, the standard deviation in the ratios of marker-specific hidden mutations was shown to be high, varying between 0.058 (for Somalia, in trios), and 0.142

(for Norway, in duos); see Table S2. Our results show that distinct levels of confidence for mutation rate estimates are expected for different markers within the same population; thus, marker-specific mutation rates should be estimated.

Furthermore, marker-specific pairwise analyses were computed, comparing the proportion of hidden mutations that were obtained for the different populations we studied; see Supplementary Material File S2. Most (98.6%, $\alpha = 0.000115$) pairwise population comparisons showed that the ratio of hidden mutations obtained for a specific marker significantly differed from population to population.

Therefore, we conclude that the difference between incompatibility rates (obtained through observations of Mendelian incompatibilities in duos or trios) and mutation rates depends on the allele frequency distribution in the population, whatever the familial configuration used (duos or trios). Globally, the markers that showed the worst and best mutation rate estimates (highest and smallest rates of hidden mutations, respectively) were D3S1358 and SE33, respectively.

None of the three populations we analyzed showed a consistent lowest value of hidden mutations across all markers, with most markers showing statistically significant pairwise differences for the rate of hidden mutations when analyzed in different populations; see Supplementary Material File S2. Nevertheless, the standard deviation associated with the marker-specific hidden mutation rates analyzed in different populations was small (maximum average $\sigma = 0.031$, see Table S3), in contrast with the one found when different markers were analyzed within a specific population (maximum average $\sigma = 0.124$; see Table S2).

Table 1. Rates of hidden mutations per marker (real and mock allelic distributions) and familial configuration considered (either duos or trios). One single-step mutation was simulated in one, randomly selected, parental meiosis of each of the 1,000,000 parent–child duos and parents–child trios, considering the allelic distributions of 10 autosomal STRs for the populations of Norway, Somalia, and Spain [34] and the allelic distributions of the 6 artificially generated markers. In the latter, N refers to the number of alleles in the marker.

Markers		Duos			Trios			
		Norway	Somalia	Spain	Norway	Somalia	Spain	
Allele Frequencies	Real allelic distributions	CSF1PO	0.546	0.497	0.497	0.269	0.219	0.207
	D1S1656	0.249	0.312	0.325	0.087	0.128	0.135	
	D21S11	0.372	0.348	0.35	0.163	0.15	0.147	
	D2S441	0.497	0.419	0.393	0.141	0.125	0.108	
	D3S1358	0.463	0.526	0.542	0.224	0.259	0.271	
	FGA	0.334	0.329	0.328	0.15	0.145	0.146	
	SE33	0.143	0.178	0.171	0.054	0.069	0.065	
	TH01	0.452	0.508	0.521	0.102	0.227	0.233	
	TPOX	0.622	0.508	0.525	0.119	0.192	0.198	
	VWA	0.445	0.425	0.435	0.213	0.205	0.205	
Mock allelic distributions	Normal (N = 10)		0.696			0.157		
	Normal (N = 20)		0.614			0.09		
	Bimodal (N = 10)		0.663			0.132		
	Bimodal (N = 20)		0.586			0.066		
	Constant (N = 10)		0.63			0.105		
	Constant (N = 20)		0.57			0.052		

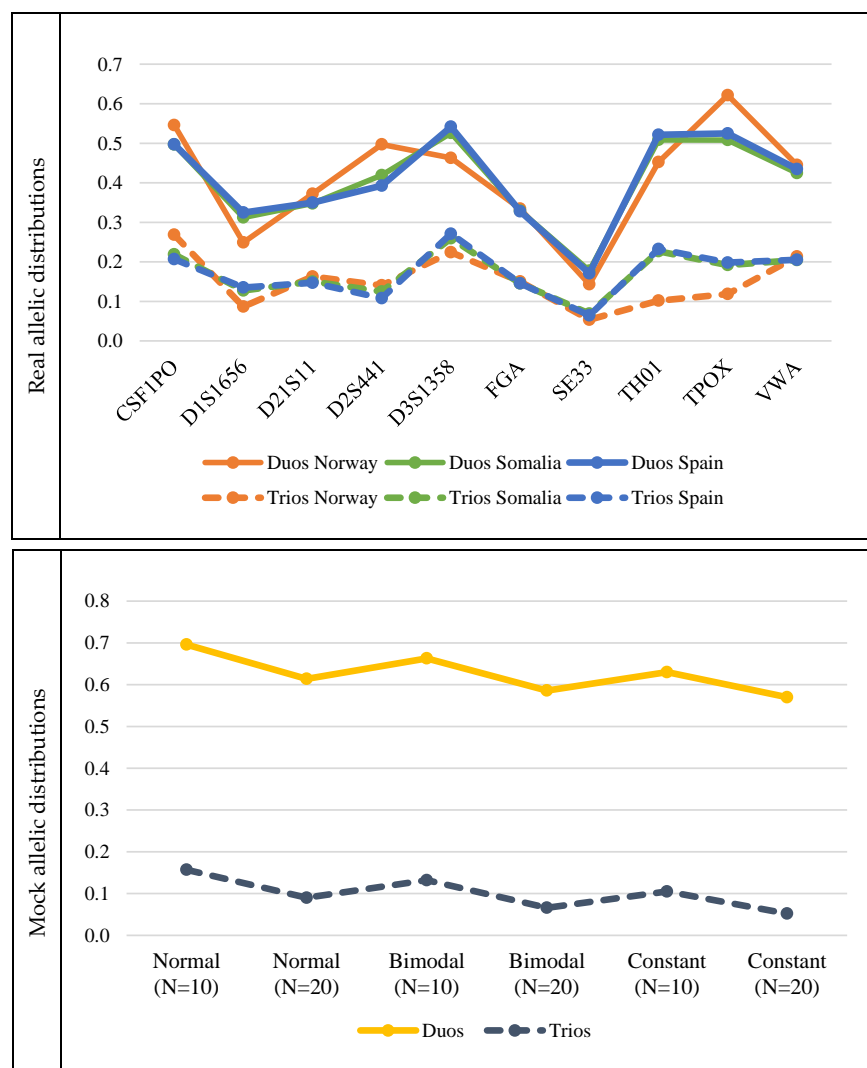


Figure 3. Graphical representations of the proportion of hidden mutations per marker (upper for real population distributions and lower for mock ones, considering the indicated distribution) and familial configuration. Full lines connect the dots corresponding to the proportion of hidden mutations for each marker in duos; dotted lines connect the dots corresponding to the proportion of hidden mutations for each marker in trios. For the mock distributions, N refers to the number of alleles considered in the marker. For example, “Normal (N = 10)” refers to the mock marker designed with a normal and narrow distribution, with 10 alleles, whereas “Normal (N = 20)” refers to the mock marker designed with a normal and wider distribution, with 20 alleles.

3.2. Mock Allele Frequency Distributions

The six mock-allelic distributions: normal (narrow and wide), bimodal (narrow and wide), and constant (narrow and wide), showed widely different proportions of hidden mutations. More specifically, in parent–child duos simulated considering the normal distribution and 10 alleles, mutations were concealed 4.4 more times than in trios. Globally, the proportion of hidden mutations varied from 52.0% (in the wide constant distribution, using trios) to 69.6% (in the narrow normal distribution, using duos). As before, our results show that distinct levels of confidence for mutation rates estimates are expected for markers with different allelic distributions, again with duos hiding more mutations than trios. Besides, markers with a narrower distribution, i.e., with fewer alleles, hid more mutations than markers with more alleles. The ratio of hidden mutations was greater when the number of alleles increased for all the analyzed distributions. For example, for a normal, unimodal distribution with 10 markers (narrow distribution), duos concealed 4.4 times more muta-

tions than trios. This figure increased to 6.8 times when 20 alleles were considered. This shows that biases resulting from the analysis of duos for estimating mutation rates via the computation of Mendelian incompatibility rates may be greater in less polymorphic populations. There is also a linear correlation between the expected heterozygosity and the rate of hidden mutations observed for the six mock allelic distributions for both duos and trios ($r^2 = 0.9841$ and $r^2 = 0.9912$, respectively); see Figure 4. Nevertheless, for the real allelic distributions that were studied, this high correlation was only verified for the case of duos ($r^2 = 0.911$; and $r^2 = 0.4609$ for trios).

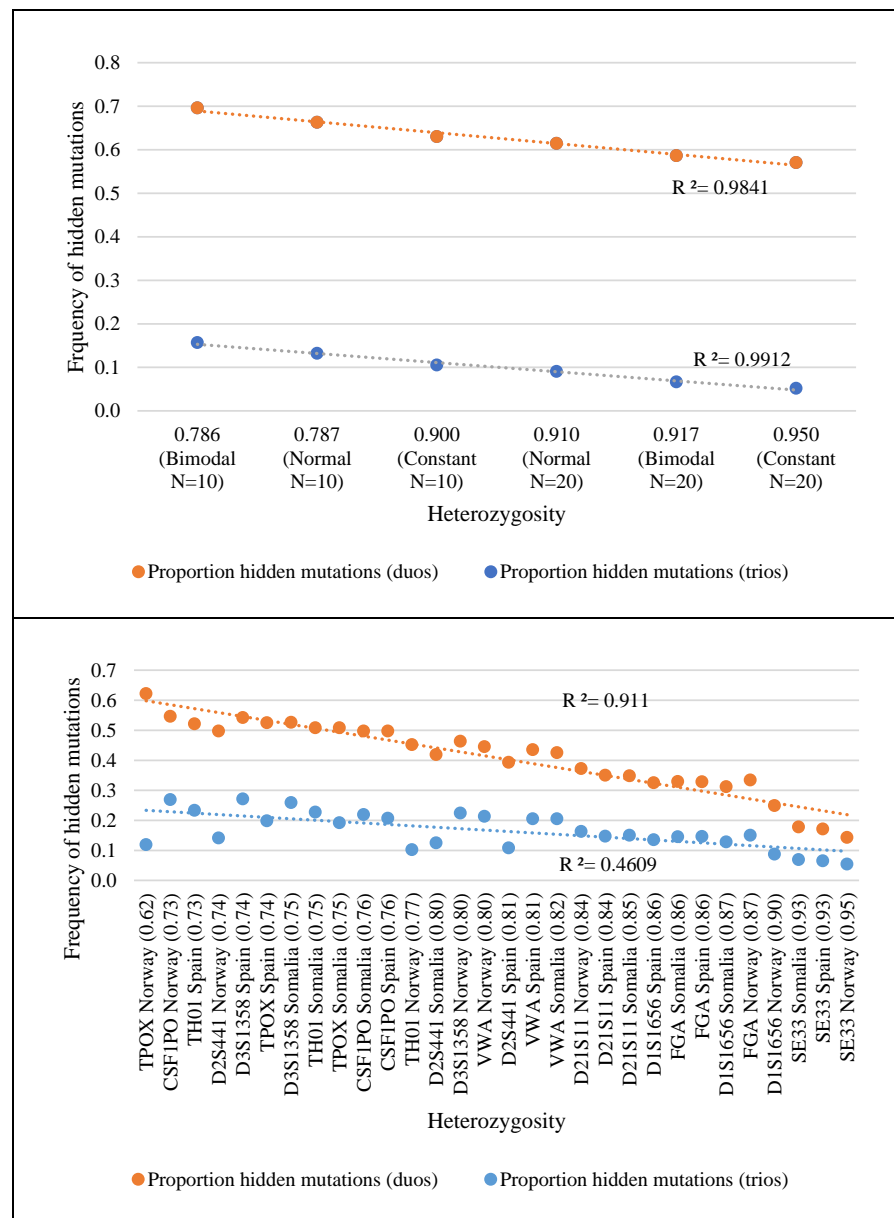


Figure 4. Graphical representations of the correlation between the frequency of hidden mutations observed per marker (upper for real population distributions and lower for mock ones, considering the indicated distribution) and markers' heterozygosity. Orange corresponds to the correlation of hidden mutations and the heterozygosity of each marker in duos, and blue in trios. For the mock distributions, N refers to the number of alleles considered in the marker. For example, “Normal (N = 10)” refers to the mock marker designed with a normal and narrow distribution, with 10 alleles, whereas “Normal (N = 20)” refers to the mock marker designed with a normal and wider distribution, with 20 alleles. Heterozygosity was calculated as $1 - \sum_i p_i^2$, where p_i is the frequency of the allele i .

4. Discussion

The accuracy of autosomal mutation rate estimates obtained through Mendelian incompatibilities varies between markers and populations according to allele frequency distributions, whatever the type of one-generation family data (parent(s)–child duos or trios) employed. Since mutations do not necessarily lead to Mendelian incompatibilities, this approach inherently underestimates their frequency.

It was previously acknowledged that the mutation rate estimates obtained through the observation of Mendelian incompatibilities at autosomal and X-chromosomal transmissions imply biases [28–31,33], and some procedures to correct them were already published for autosomal transmission [29–31,33]. Despite this, the generally accepted approach continues to be the direct estimation of mutation rates through the counting of Mendelian incompatibilities, without any correction; see, for example [24–27,35–38].

In autosomes, biases are more important in parent–child duos than in trios [29], showing that pooling data from the two types of sources is not acceptable, as it prevents any kind of a posteriori correction.

We have demonstrated that the probability of the occurrence of hidden mutations depends on the allele frequency distribution; therefore, the same marker may show different estimates in distinct populations despite the mutation rate value being the same. At this point, it should be highlighted that the real frequency distributions available for our analyses correspond to the markers designed for forensic individual identification, comprising STRs with a high diversity within, rather than between, populations. This is not the case for markers of anthropological interest, which were selected to maximize the differences between populations. In this case, pooling data from different populations to estimate mutation rates should be carefully thought out and planned, as different allelic distributions carry different likelihoods of disclosing mutations.

The framework we present in this work, described in the Materials and Methods section and thoroughly explained in <https://github.com/econdesousa/Incomp2Mut.git> (accessed on 23 March 2022), can be used to correct the mutation rates estimated through the MIA. To obtain the proposed corrective factor, it is only necessary to know the distribution of the allele frequencies at the loci of interest, the incompatibility rate observed and whether duos or trios were used to ascertain said rate. The output will be the corrected (for hidden mutations) mutation rate for the analyzed microsatellite. As exemplified, if parent–child duos are used and an R rate of Mendelian incompatibilities is found at the CSF1PO locus in the Norwegian population, the corrected value of $R/(1-0.546)$ should be used as the estimated mutation rate at this locus and population, which represents nearly double the value estimated via MIA.

5. Conclusions

The accuracy of microsatellite mutation rate estimates obtained through the observation of Mendelian incompatibilities in parent(s)–child duos or trios depends on several factors, including the population allele frequency distribution. We showed that even when trios are used, as many as 27.1% (as obtained for marker D3S1358 for the population of Spain) of the mutations did not lead to any incompatibility. Although we framed our analyses under the knowledge that single-step mutations are the most frequent, the magnitude and the types of the biases increase if other mutations are considered (data not shown). We also did not consider the causes of the evidenced differences in the estimates across populations, i.e., whether biases are due to simple statistical properties of allelic distributions or intrinsic differences in allelic mutability. Whatever the reasons for these differences, its effect is the same on the estimation accuracy, as it only depends on the allele frequency distribution. However, the long-term evolutionary consequences are different. It is also important to note that population differentiation is expected to be lower for autosomal than for heterosomal markers, which are more susceptible to genetic drift. Therefore, the variation observed in the frequency of hidden mutations among populations when using autosomal markers may be even higher for heterosomal microsatellites.

The impact of this systematic underestimation inherent to the approach can be particularly burdensome in crucial anthropological problems, such as when dating evolutionary events; see, for example, [6,7,10].

We propose a simple method to obtain mutation rate estimates from Mendelian incompatibilities when using familial duos or trios, aiming to minimize the impact of hidden mutations. An informatics tool is provided at <https://github.com/econdesousa/Incomp2Mut.git> (accessed on 23 March 2022) to replicate this approach and obtain corrected mutation rates for any autosomal microsatellite, employing the allele frequency distribution and incompatibility rate estimated for either duos or trios.

Supplementary Materials: The following supporting information can be downloaded at: <https://www.mdpi.com/article/10.3390/genes13071248/s1>, Supplementary Material File S1: Allelic distribution of marker CSF1PO for the populations of Norway (N = 19,156), Somalia (N = 1598) and Spain (N = 2500); Supplementary Material File S2: *p* values found in pairwise comparisons between the frequency of hidden mutations found when one-step mutation is simulated in parents-child trios for each marker and population. Table S1: Population size (N), expected heterozygosity (with Nei correction), polymorphic informative content (PIC), number of alleles and allelic range per marker and population; Table S2: Populations showing the highest and lowest standard deviations (σ between parentheses) considering the proportion of hidden mutations across markers, for each familial configuration type. A single-step mutation was simulated in one of the parental meiosis of 1,000,000 configurations of each type, considering the allele frequencies of 10 autosomal STRs in three populations (Norway, Somalia, and Spain); Table S3: Average standard deviation and markers showing the highest and lowest values (in parentheses) of the proportion of hidden mutations across the different population databases: Norway, Somalia, and Spain, for each familial configuration type. A single-step mutation was simulated in one of the parental meiosis of 1,000,000 configurations of each type, considering the allele frequencies of 10 autosomal STRs in three populations (Norway, Somalia, and Spain).

Author Contributions: Conceptualization, L.G., A.A. and N.P.; Data curation, S.A.-S., E.C.-S. and N.P.; Formal analysis, S.A.-S., E.C.-S., L.G., A.A. and N.P.; Funding acquisition, S.A.-S., E.C.-S., L.G., A.A. and N.P.; Investigation, S.A.-S., E.C.-S., L.G., A.A. and N.P.; Methodology, S.A.-S., E.C.-S., L.G., A.A. and N.P.; Software, S.A.-S., E.C.-S. and N.P.; Supervision, L.G., A.A. and N.P.; Validation, S.A.-S., E.C.-S., L.G., A.A. and N.P.; Writing—original draft, S.A.-S.; Writing—review and editing, S.A.-S., E.C.-S., L.G., A.A. and N.P. All authors have read and agreed to the published version of the manuscript.

Funding: FEDER—Fundo Europeu de Desenvolvimento Regional funds through the COMPETE 2020—Operacional Programme for Competitiveness and Internationalisation (POCI), Portugal 2020; FCT—Fundação para a Ciência e Tecnologia: projects “Institute for Research and Innovation in Health Sciences” (POCI-01-0145-FEDER-007274); FCT—Fundação para a Ciência e Tecnologia: Decree-Law no.57/2016 of August 29; FCT—Fundação para a Ciência e Tecnologia: SFRH/BD/136284/2018; CNPq—National Council for Scientific and Technological Development: ref. 306342/2019-7; FAPERJ—Fundação de Amparo à Pesquisa do Estado do Rio de Janeiro: (CNE-2018); i3S—Instituto de Investigação e Inovação em Saúde, Universidade do Porto, Portugal: POCI-01-0145-FEDER-007274; CMUP—Center of Mathematics of the University of Porto: UIDB/00144/2020; PPBI—Portuguese Platform of BioImaging: PPBI-POCI-01-0145-FEDER-022122.

Institutional Review Board Statement: Not applicable.

Informed Consent Statement: Not applicable.

Data Availability Statement: Not applicable.

Conflicts of Interest: The authors declare no conflict of interest.

References

1. Flores-Espinoza, R.; Paz-Cruz, E.; Ruiz-Pozo, V.A.; Lopez-Carrera, M.; Cabrera-Andrade, A.; Gusmão, L.; Burgos, G. Investigating genetic diversity in admixed populations from Ecuador. *Am. J. Phys. Anthropol.* **2021**, *176*, 109–119. [[CrossRef](#)]
2. Srithawong, S.; Muisuk, K.; Srikumool, M.; Kampuansai, J.; Pittayaporn, P.; Ruangchai, S.; Liu, D.; Kutanan, W. Close genetic relationship between central Thai and Mon people in Thailand revealed by autosomal microsatellites. *Int. J. Leg. Med.* **2021**, *135*, 445–448. [[CrossRef](#)] [[PubMed](#)]
3. He, G.; Wang, Z.; Wang, M.; Hou, Y. Genetic Diversity and Phylogenetic Differentiation of Southwestern Chinese Han: A comprehensive and comparative analysis on 21 non-CODIS STRs. *Sci. Rep.* **2017**, *7*, 13730. [[CrossRef](#)] [[PubMed](#)]
4. Sun, J.X.; Mullikin, J.C.; Patterson, N.; Reich, D.E. Microsatellites are molecular clocks that support accurate inferences about history. *Mol. Biol. Evol.* **2009**, *26*, 1017–1027. [[CrossRef](#)] [[PubMed](#)]
5. Peixoto, A.; Santos, C.; Pinheiro, M.; Pinto, P.; Soares, M.J.; Rocha, P.; Gusmão, L.; Amorim, A.; Van Der Hout, A.; Gerdes, A.-M.; et al. International distribution and age estimation of the Portuguese BRCA2 c.156_157insAlu founder mutation. *Breast Cancer Res. Treat.* **2011**, *127*, 671–679. [[CrossRef](#)]
6. Sharony, R.; Martins, S.; Costa, I.P.D.; Zaltzman, R.; Amorim, A.; Sequeiros, J.; Gordon, C.R. Yemenite-Jewish families with Machado-Joseph disease (MJD/SCA3) share a recent common ancestor. *Eur. J. Hum. Genet.* **2019**, *27*, 1731. [[CrossRef](#)]
7. Martins, S.; Soong, B.-W.; Wong, V.C.N.; Giunti, P.; Stevanin, G.; Ranum, L.P.W.; Sasaki, H.; Riess, O.; Tsuji, S.; Coutinho, P.; et al. Mutational origin of Machado-Joseph disease in the Australian Aboriginal communities of Groote Eylandt and Yirrkala. *Arch. Neurol.* **2012**, *69*, 746–751. [[CrossRef](#)]
8. Martins, S.; Calafell, F.; Gaspar, C.; Wong, V.C.N.; Silveira, I.; Nicholson, G.A.; Brunt, E.R.; Tranebjaerg, L.; Stevanin, G.; Hsieh, M.; et al. Asian origin for the worldwide-spread mutational event in Machado-Joseph disease. *Arch. Neurol.* **2007**, *64*, 1502–1509. [[CrossRef](#)]
9. Boattini, A.; Sarno, S.; Mazzarisi, A.M.; Viroli, C.; De Fanti, S.; Bini, C.; Larmuseau, M.H.D.; Pelotti, S.; Luiselli, D. Estimating Y-Str Mutation Rates and TmrcA Through Deep-Rooting Italian Pedigrees. *Sci. Rep.* **2019**, *9*, 9032. [[CrossRef](#)]
10. Rigueiro, M.; Alvarez, J.; Rowold, D.; Herrera, R.J. On the origins, rapid expansion and genetic diversity of Native Americans from hunting-gatherers to agriculturalists. *Am. J. Phys. Anthropol.* **2013**, *150*, 333–348. [[CrossRef](#)]
11. Strand, M.; Prolla, T.A.; Liskay, R.M.; Petes, T.D. Destabilization of tracts of simple repetitive DNA in yeast by mutations affecting DNA mismatch repair. *Nature* **1993**, *365*, 274–276. [[CrossRef](#)] [[PubMed](#)]
12. Schlötterer, C.; Tautz, D. Slippage synthesis of simple sequence DNA. *Nucleic Acids Res.* **1992**, *20*, 211. [[CrossRef](#)] [[PubMed](#)]
13. Eckert, K.A.; Hile, S.E. Every microsatellite is different: Intrinsic DNA features dictate mutagenesis of common microsatellites present in the human genome. *Mol. Carcinog.* **2009**, *48*, 379–388. [[CrossRef](#)]
14. Wierdl, M.; Dominska, M.; Petes, T.D. Microsatellite instability in yeast: Dependence on the length of the microsatellite. *Genetics* **1997**, *146*, 769–779. [[CrossRef](#)] [[PubMed](#)]
15. Brinkmann, B.; Klintschar, M.; Neuhuber, F.; Hühne, J.; Rolf, B. Mutation Rate in Human Microsatellites: Influence of the Structure and Length of the Tandem Repeat. *Am. J. Hum. Genet.* **1998**, *62*, 1408–1415. [[CrossRef](#)]
16. Ballantyne, K.N.; Goedbloed, M.; Fang, R.; Schaap, O.; Lao, O.; Wollstein, A.; Choi, Y.; van Duijn, K.; Vermeulen, M.; Brauer, S.; et al. Mutability of Y-Chromosomal Microsatellites: Rates, Characteristics, Molecular Bases, and Forensic Implications. *Am. J. Hum. Genet.* **2010**, *87*, 341. [[CrossRef](#)]
17. Sun, J.X.; Helgason, A.; Masson, G.; Ebenesersdóttir, S.S.; Li, H.; Mallick, S.; Gnerre, S.; Patterson, N.; Kong, A.; Reich, D.; et al. A direct characterization of human mutation based on microsatellites. *Nat. Genet.* **2012**, *44*, 1161–1165. [[CrossRef](#)]
18. Xu, X.; Peng, M.; Fang, Z.; Xu, X. The direction of microsatellite mutations is dependent upon allele length. *Nat. Genet.* **2000**, *24*, 396–399. [[CrossRef](#)]
19. Weber, J.L.; Wong, C. Mutation of human short tandem repeats. *Hum. Mol. Genet.* **1993**, *2*, 1123–1128. [[CrossRef](#)]
20. Kimura, M.; Ohta, T. Stepwise mutation model and distribution of allelic frequencies in a finite population. *Proc. Natl. Acad. Sci. USA* **1978**, *75*, 2868. [[CrossRef](#)]
21. Pinto, N.; Gusmão, L.; Amorim, A. Mutation and mutation rates at y chromosome specific Short Tandem Repeat Polymorphisms (STRs): A reappraisal. *Forensic Sci. Int. Genet.* **2014**, *9*, 20–24. [[CrossRef](#)] [[PubMed](#)]
22. Antão-Sousa, S.; Sánchez-Diz, P.; Abovich, M.; Alvarez, J.; Carvalho, E.; Silva, C.; Domingues, P.; Farfán, M.; Gutierrez, A.; Pontes, L.; et al. Mutation rates and segregation data on 16 Y-STRs: An update to previous GHEP-ISFG studies. *Forensic Sci. Int. Genet. Suppl. Ser.* **2017**, *6*, e601–e602. [[CrossRef](#)]
23. Dupuy, B.M.; Stenersen, M.; Egeland, T.; Olaisen, B. Y-chromosomal microsatellite mutation rates: Differences in mutation rate between and within loci. *Hum. Mutat.* **2004**, *23*, 117–124. [[CrossRef](#)] [[PubMed](#)]
24. Jin, B.; Su, Q.; Luo, H.; Li, Y.; Wu, J.; Yan, J.; Hou, Y.; Liang, W.; Zhang, L. Mutational analysis of 33 autosomal short tandem repeat (STR) loci in southwest Chinese Han population based on trio parentage testing. *Forensic Sci. Int. Genet.* **2016**, *23*, 86–90. [[CrossRef](#)] [[PubMed](#)]
25. Pinto, N.; Pereira, V.; Mas, C.T.; Loiola, S.; Carvalho, E.F.; Modesti, N.; Maxzud, M.; Marcucci, V.; Cano, H.; Cicarelli, R.; et al. Paternal and maternal mutations in X-STRs: A GHEP-ISFG collaborative study. *Forensic Sci. Int. Genet.* **2020**, *46*, 102258. [[CrossRef](#)]
26. García, M.G.; Catanesi, C.I.; Penacino, G.A.; Gusmão, L.; Pinto, N. X-chromosome data for 12 STRs: Towards an Argentinian database of forensic haplotype frequencies. *Forensic Sci. Int. Genet.* **2019**, *41*, e8–e13. [[CrossRef](#)]

27. Sun, H.; Liu, S.; Zhang, Y.; Whittle, M.R. Comparison of southern Chinese Han and Brazilian Caucasian mutation rates at autosomal short tandem repeat loci used in human forensic genetics. *Int. J. Leg. Med.* **2014**, *128*, 1–9. [[CrossRef](#)]
28. Antão-Sousa, S.; Conde-Sousa, E.; Gusmão, L.; Amorim, A.; Pinto, N. Underestimation and misclassification of mutations at X chromosome STRs depend on population's allelic profile. *Forensic Science International: Genet. Suppl. Ser.* **2019**, *7*, 718–720. [[CrossRef](#)]
29. Slooten, K.; Ricciardi, F. Estimation of mutation probabilities for autosomal STR markers. *Forensic Sci. Int. Genet.* **2013**, *7*, 337–344. [[CrossRef](#)]
30. Chakraborty, R.; Stivers, D.N.; Zhong, Y. Estimation of mutation rates from parentage exclusion data: Applications to STR and VNTR loci. *Mutat. Res.* **1996**, *354*, 41–48. [[CrossRef](#)]
31. Vicard, P.; Dawid, A.P. A statistical treatment of biases affecting the estimation of mutation rates. *Mutat. Res.* **2004**, *547*, 19–33. [[CrossRef](#)] [[PubMed](#)]
32. Brenner, C.H. Multiple mutations, covert mutations and false exclusions in paternity casework. *Int. Congr. Ser.* **2004**, *1261*, 112–114. [[CrossRef](#)]
33. Vicard, P.; Dawid, A.P.; Mortera, J.; Lauritzen, S.L. Estimating mutation rates from paternity casework. *Forensic Sci. Int. Genet.* **2008**, *2*, 9–18. [[CrossRef](#)]
34. Kling, D.; Tillmar, A.O.; Egeland, T. Familias 3—Extensions and new functionality. *Forensic Sci. Int. Genet.* **2014**, *13*, 121–127. [[CrossRef](#)] [[PubMed](#)]
35. Lan, Q.; Wang, H.; Shen, C.; Guo, Y.; Yin, C.; Xie, T.; Fang, Y.; Zhou, Y.; Zhu, B. Mutability analysis towards 21 STR loci included in the AGCU 21 + 1 kit in Chinese Han population. *Int. J. Leg. Med.* **2018**, *132*, 1287–1291. [[CrossRef](#)] [[PubMed](#)]
36. Liu, Q.L.; Chen, Y.F.; Huang, X.L.; Liu, K.Y.; Zhao, H.; Lu, D.J. Population data and mutation rates of 19 STR loci in seven provinces from China based on Goldeneye™ DNA ID System 20A. *Int. J. Leg. Med.* **2017**, *131*, 653–656. [[CrossRef](#)] [[PubMed](#)]
37. Hongdan, W.; Bing, K.; Ning, S.; Miao, H.; Bo, Z.; Yuxin, G.; Bofeng, Z.; Shixiu, L.; Zhaoshu, Z. Evaluation of the genetic parameters and mutation analysis of 22 STR loci in the central Chinese Han population. *Int. J. Leg. Med.* **2017**, *131*, 103–105. [[CrossRef](#)]
38. Zhao, Z.; Zhang, J.; Wang, H.; Liu, Z.-P.; Liu, M.; Zhang, Y.; Sun, L.; Zhang, H. Mutation rate estimation for 15 autosomal STR loci in a large population from Mainland China. *Meta Gene* **2015**, *5*, 150–156. [[CrossRef](#)]